ACS SENSORS

pubs.acs.org/acssensors Article

Development of an miRFP680-Based Fluorescent Calcium Ion Biosensor Using End-Optimized Transposons

Fu Chai, Hajime Fujii, Giang N. T. Le, Chang Lin, Keisuke Ota, Karl Matthew Lin, Lam M. T. Pham, Peng Zou, Mikhail Drobizhev, Yusuke Nasu, Takuya Terai, Haruhiko Bito, and Robert E. Campbell*

Cite This: *ACS Sens.* 2024, 9, 3394−3402 Read Online

ACCESS | Metrics & More | Article Recommendations | Supporting Information

ABSTRACT: The development of new or improved single fluorescent protein (FP)-based biosensors (SFPBs), particularly those with excitation and emission at near-infrared wavelengths, is important for the continued advancement of biological imaging applications. In an effort to accelerate the development of new SFPBs, we report modified transposons for the transposase-based creation of libraries of FPs randomly inserted into analyte binding domains, or vice versa. These modified transposons feature ends that are optimized to minimize the length of the linkers that connect the FP to the analyte binding domain. We rationalized that shorter linkers between the domains should result in more effective allosteric coupling between the analyte binding-dependent conformational change in the binding domain and the fluorescence modulation of the chromophore of the FP domain. As a proof of concept, we employed end-modified Mu transposons for the discovery of SFPB prototypes based on the insertion of two circularly permuted red FPs (mApple and FusionRed) into binding proteins for L-lactate and spermidine. Using an analogous approach, we discovered calcium ion (Ca^{2+})-specific SFPBs by random insertion of calmodulin (CaM)-RS20 into miRFP680, a particularly bright near-infrared (NIR) FP based on a biliverdin (BV)-binding fluorescent protein. Starting from an miRFP680-based Ca^{2+} biosensor prototype, we performed extensive directed evolution, including under BV-deficient conditions, to create highly optimized biosensors designated the NIR-GECO3 series. We have extensively characterized the NIR-GECO3 series and explored their utility for biological Ca^{2+} imaging. The methods described in this work will serve to accelerate SFPB development and open avenues for further exploration and optimization of SFPBs across a spectrum of biological applications.

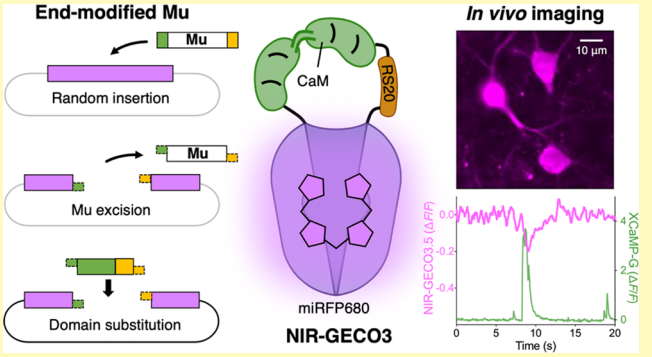

KEYWORDS: *fluorescence microscopy, cell signaling, protein engineering, directed evolution, transposons, biliverdin-binding fluorescent protein, heme oxygenase*

Single fluorescent protein-based biosensors (SFPBs) represent one of the most impactful and widely used classes of tools for minimally invasive biological imaging.[1,2] SFPBs are fully genetically encoded and consist of a fluorescent protein (FP) domain that is allosterically linked to an analyte-specific binding domain.[3] Analyte binding elicits a conformational change that is propagated to the FP domain. This, in turn, alters the microenvironment surrounding the FP's chromophore, leading to a modulation of the fluorescence intensity that can be readily visualized in cultured tissues or in vivo using fluorescence microscopy. Prototype or poorly optimized SFPBs could have analyte-dependent fluorescent intensity changes ($\Delta F/F_{min} = (F_{max} - F_{min})/F_{min}$) of less than one, which can complicate cell imaging due to small signal-to-noise ratios (SNR). In contrast, highly optimized, high-performance biosensors typically have higher SNR due to fluorescence changes of greater than 10 or, in rare cases, greater than 100.[4]

Development of a new SFPB usually commences with the discovery of a prototype in which an allosteric connection between the FP and binding domains has been established. Discovery of such prototypes is often a rate-limiting step in SFPB development. Traditionally, a common approach for the discovery of prototypes is the manual one-at-a-time construction of a large number of variants in which the FP domain

Received: March 29, 2024
Revised: May 14, 2024
Accepted: May 17, 2024
Published: June 1, 2024

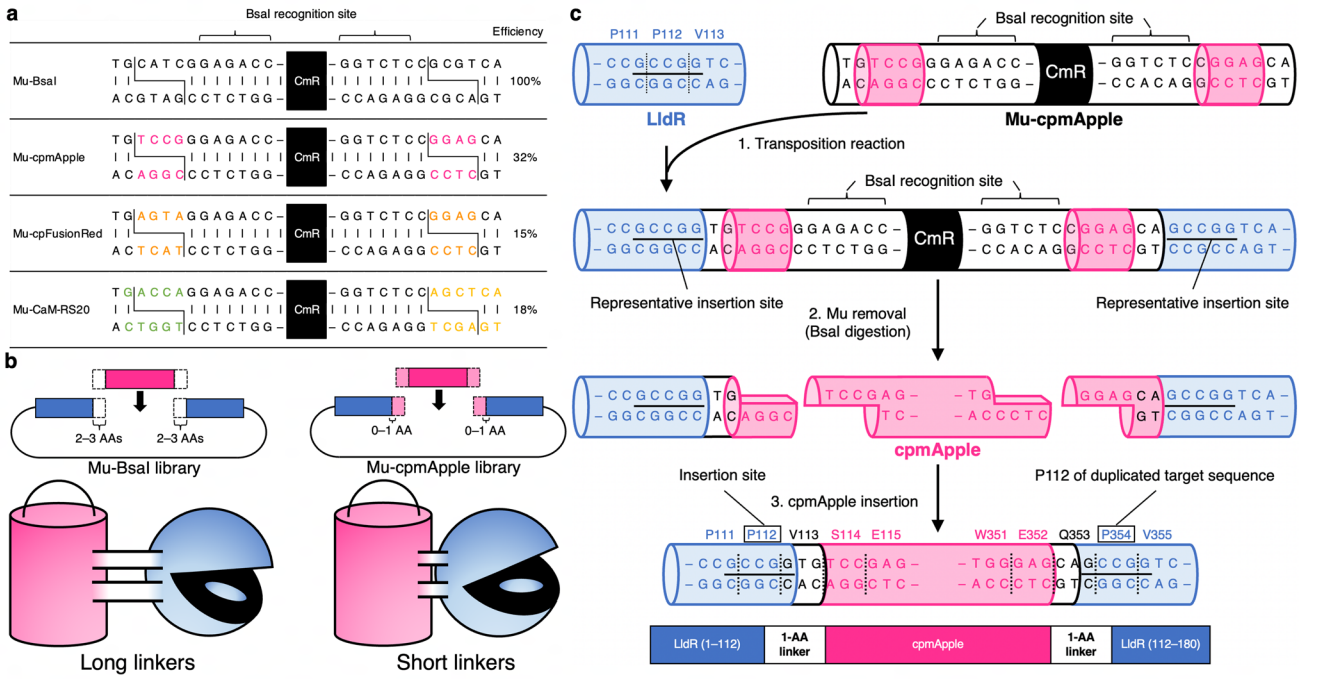

Figure 1. Generation of linker-shortened libraries using end-modified Mu transposons. (a) Sequences of the end-modified Mu transposon ends, presented with the top strand in the 5′ to 3′ orientation. The chloramphenicol resistance gene (CmR) is shown in black. The efficiency of each end-modified transposon was calculated by comparing colony number, relative to Mu-BsaI, in the primary library. (b) Schematic representation of linker lengths in both the plasmid (above) and the protein structure (below). The target domain is depicted in blue, and the inserted domain is in red. "AA" stands for amino acids. (c) Schematic representation of key steps in the assembly of cpmApple-inserted LldR-LBD libraries. Colors are consistent with panels (a) and (b). Integration of Mu-cpmApple results in a 5 base pair duplication at the target site (underscored). In the representative example shown, P112 is identified as the insertion site, and V113 and Q353 are considered as "linkers" between cpmApple and LldR-LBD.

is inserted into the binding domain, connected via short linkers. The sites of insertion would typically be locations that are known to undergo conformational changes upon analyte binding, and various other solvent-exposed sites within the binding domain. A functional allosteric connection depends on two aspects: the site at which one domain is inserted into the other, and the proximity between the two domains which is determined by the linker length.

High-throughput library generation and screening are emerging as an alternative approach to manual one-at-a-time construction and testing of SFPB prototypes. For example, Nadler et al. reported a Mu transposon-based method which enabled the rapid construction of an SFPB library with all possible insertions of one domain into another (Figure S1a).[5] Complementing such molecular biology methods are massively parallel assays that can be used to screen large SFPB variant libraries based on fluorescence changes in response to the analyte of interest. One example is sort-seq which combines fluorescence-activated cell sorting (FACS) with deoxyribonucleic acid (DNA) sequencing.[5−7] Whatever the screening method, to maximize the chances of finding a highly effective biosensor prototype, it is ideal to have minimal length linkers connecting the binding domain to the FP domain. In the work of Nadler et al., the transposons were designed to leave minimal remnant "scars" (i.e., linkers) flanking the site of transposon insertion, but linkers of 2−3 amino acids were typical (Figure S1b). If these linkers could be further shortened, we suspect that SFPB prototypes with greater potential for conversion into high-performance biosensors could be discovered.[3]

In this work, we describe the development of end-modified Mu transposons to facilitate the identification of SFPB prototypes with shorter linkers between the FP and binding domains. As a proof of concept, we have applied these transposons for the development of SFPB prototypes based on the mApple and FusionRed red fluorescent proteins (RFPs) combined with L-lactate- and spermidine-binding proteins. Furthermore, we applied a similar approach to identify an SFPB prototype consisting of a calcium ion (Ca^{2+})-binding domain inserted into the miRFP680 near-infrared (NIR) FP. Extensive directed evolution and optimization of this latter construct ultimately resulted in a new series of NIR fluorescent Ca^{2+} biosensors, designated the NIR-GECO3 series. We demonstrate the potential utility of the NIR-GECO3 series for Ca^{2+} imaging in cultured cells and in live mice.

RESULTS AND DISCUSSION

End-Modified Mu Transposons for Insertion of cpmApple and cpFusionRed. Positioning of the FP domain in close proximity to the analyte binding domain, through the use of minimal linker lengths, is a prerequisite for producing functional allostery in an SFPB. Indeed, minimization of the linker length has been suggested as an effective strategy at the earliest stages of SFPB engineering.[3,8] Based on this rationale, we aimed to modify the ends of the Mu transposon in order to produce the shortest possible linkers. Nadler et al. demonstrated that the ends of the Mu transposon, which includes an antibiotic resistance marker for the selection of plasmids into which the transposon has been inserted, can be modified to incorporate enzyme restriction sites for later excision and

https://doi.org/10.1021/acssensors.4c00727
ACS Sens. 2024, 9, 3394−3402

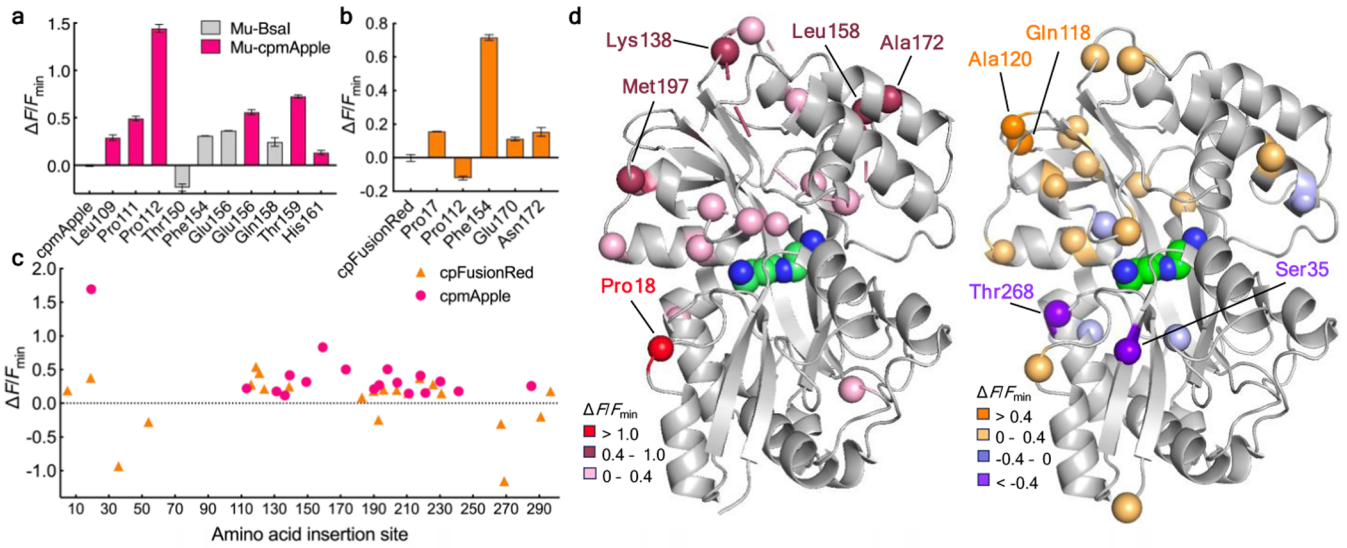

Figure 2. Characterization of LldR-LBD and PotD Libraries with cpRFP Insertions. (a) Fluorescence change ($\Delta F/F_{min}$) of variants from cpmApple-inserted LldR-LBD libraries in response to 10 mM L-lactate in screening buffers. Negative $\Delta F/F_{min}$ values indicate an inverse response. Error bars represent ± standard deviation (n = 3). (b) $\Delta F/F_{min}$ values of variants from the cpFusionRed-inserted LldR-LBD library, represented as in (a). (c) Distribution of $\Delta F/F_{min}$ values for functional insertions along the PotD sequence in response to 10 mM spermidine in screening buffers. (d) Positions of insertions (spheres) for functional cpmApple (left) and cpFusionRed (right) insertions into PotD (PDB 1POY).[18] Spermidine is shown in a sphere representation (carbon in green and nitrogen in blue).

replacement with an FP domain (Figure S1).[5] This method maintains the integrity of motifs within the Mu termini which are essential for efficient transposition, while allowing for the shortening of the length of the remnant scars. We rationalized that the linkers could be further shortened by creating an end-modified Mu transposon that already incorporated the N- and C-terminal sequences of the specific FP domain that would be inserted at a later stage (Figure 1).

To create appropriately end-modified Mu transposons, we modified Nadler et al.'s Mu transposon with BsaI cut sites (hereinafter referred to as Mu-BsaI) by site-directed mutagenesis (Figure 1a).[5] BsaI is a type IIS restriction enzyme that cleaves outside of its recognition sequence. Taking advantage of this property, we exchanged the N- and C-terminal cleavage sites of Mu-BsaI with the N- and C-terminal sequences, respectively, of specific FP. Accordingly, a transposon was designed for each of the two circularly permuted (cp) red fluorescent proteins (cpRFPs) used in this work: cpmApple[9] and cpFusionRed[10] (Table S1). The Mu-cpmApple transposon was designed with cut site sequences flanking the "gate post" residues of mApple, Ser146, and Glu143 (mApple numbering).[3] The Mu-cpFusionRed transposon was similarly designed with cut sites flanking Ser143 and Glu141 (FusionRed numbering). At the 5′ end of the BsaI recognition site, there is a TG dinucleotide that is strictly conserved and could therefore not be replaced.[11] In the end-optimized transposons, this TG sequence is followed by the first four (at the N-terminal end) or the last four (at the C-terminal end) of the cpRFP. Including four nucleotides ensures that the reading frame is maintained when the cpRFP is inserted into the target binding domain. This strategy should result in minimal linker lengths on both sides of the inserted domain (Figure 1b,c). Notably, insertion in only one of the three possible reading frames will result in the correct translation of the inserted cpRFP domain (Figure S2).

A potential limitation of this approach is that, for each variant in the library, there is only one N- and one C-terminal linker sequence being tested and the sequence of this linker depends on the insertion site. For insertion in the correct reading frame, the conserved TG dinucleotide is in the second and third positions of the N-terminal linker codon (i.e., codon NTG, where N = A, G, C, or T), and its reverse complement (CA) is in the first and second positions of the C-terminal linker codon (i.e., codon CAN) (Figure S2). Accordingly, only Leu, Met, or Val can be the N-terminal linker and only His or Gln can be C-terminal linker. This means that we are certainly missing promising sites that might only be tolerated, or might give a larger fluorescent response, with a different linker sequence. Keeping this limitation in mind, the main goal of this approach is to identify sites that are tolerant of insertion and give enough of an analyte-dependent fluorescent change, with minimal linkers, to suggest that further engineering by linker optimization and directed evolution might be worthwhile.

Transposon-Based Random Insertion of cpmApple into a Lactate-Binding Protein. Libraries were constructed to demonstrate the feasibility of random cpmApple insertions within the L-lactate-binding domain (LBD) of the *Escherichia coli* (*E. coli*) LldR transcriptional regulator,[12] utilizing both the original Mu-BsaI and the modified Mu-cpmApple transposons (Figure 1c). We previously used LldR-LBD as a binding domain to engineer a high-performance SFPB for L-lactate.[13] Random incorporation of cpmApple into LldR-LBD was verified through DNA sequencing (Figure S3). The transposon-based library construction strategy relies on the random insertion of the Mu sequence throughout the LldR-LBD in all six reading frames. Mu is subsequently replaced with the cpmApple sequence using BsaI digestion and DNA ligation (that is, using Golden Gate assembly). To mitigate growth bias in the libraries, the initially generated plasmid DNA library was used to transform *E. coli* that was then grown on Luria−Bertani (LB) agar plates supplemented with appropriate antibiotics, harvested by scraping, and processed for DNA extraction. For this initial step (i.e., the transposon reaction performed on a plasmid encoding LldR-LBD), the number of independent

https://doi.org/10.1021/acssensors.4c00727
ACS Sens. 2024, 9, 3394−3402

clones was greater than 10× the total number of nucleotides in the plasmid. Subsequent steps included: excision of the LldR-LBD region, gel purification of the band corresponding to LldR-LBD plus a single Mu transposon, ligation into a bacterial expression plasmid, and replacement of the transposon with the gene encoding the rest of cpmApple (similar to Figure S1a).

Screening of Libraries with Random Insertion of cpmApple into a Lactate-Binding Protein. Following cpmApple insertion, *E. coli* was transformed with libraries (Mu-BsaI and Mu-cpmApple) and >30,000 colonies (at least 30× the number of nucleotides (540) encoding LldR-LBD) of each library were assessed for fluorescence using a custom-built colony screener. Approximately 5−10% of the variants in the final library selection exhibited fluorescence. Colonies displaying the brightest fluorescence were cultured and their respective proteins were tested for in vitro functionality in a 96-well plate format (Figure S4). Using a detergent-based reagent (B-PER), we extracted proteins and quantified $\Delta F/F_{min}$ in response to 10 mM L-lactate. We examined seven 96-well plates for each library, representing over three times the theoretical number of insertion variants (equal to the number of amino acids (180) encoding LldR-LBD). In the initial screening phase, 84 variants from each library exhibiting bright fluorescence and/or large $\Delta F/F_{min}$ in response to L-lactate were selected for further characterization.

As a secondary assay, we performed triplicate measurements of each variant in the presence and absence of 10 mM L-lactate. Notably, a subset of cpmApple insertion variants from both the Mu-BsaI and Mu-cpmApple libraries exhibited substantial $\Delta F/F_{min}$ (Figures 2a, S5a, and Table S2). To simplify this discussion, we do not distinguish between direct response (increased fluorescence upon L-lactate addition) and inverse response (decreased fluorescence upon L-lactate addition). In the Mu-BsaI library, cpmApple insertions at positions Phe154 ($\Delta F/F_{min}$ = 0.31), Glu156 ($\Delta F/F_{min}$ = 0.36), and Gln158 ($\Delta F/F_{min}$ = 0.25) of LldR-LBD exhibited substantial responses (Figure S6a). Variants identified from the Mu-cpmApple library, including Pro112 ($\Delta F/F_{min}$ = 1.44), Glu156 ($\Delta F/F_{min}$ = 0.56), and Thr159 ($\Delta F/F_{min}$ = 0.73, dissociation constant (K_d) = 0.27 mM), tended to exhibit larger responses than those from the Mu-BsaI library, suggesting that the use of short linkers may result in more effective allosteric connections (Figure S6b and Table S3). A clustering of insertions at Leu109, Pro111, and Pro112 suggests that these positions may be a promising and permissive hotspot for the generation of SFPBs (Figure S7). Insertions in the vicinity of this hotspot were previously used to generate the iLACCO1 and R-iLACCO1 L-lactate SFPBs which both have the cpFP inserted after Leu109 of the LldR-LBD.[13,14] In the previous work, candidate insertion sites in solvent-exposed loops were identified by manual inspection of the computationally predicted structure and then tested one by one.

Random Insertions of cpFusionRed into a Lactate-Binding Protein. The use of Mu-cpFusionRed transposons also enabled the random insertion of cpFusionRed into LldR-LBD. Screening this library led to the identification of several functional variants within regions also identified from the Mu-cpmApple library. Insertions with notable fluorescence changes upon L-lactate addition included Phe154 ($\Delta F/F_{min}$ = 0.72, K_d = 1.4 mM) and Pro112 ($\Delta F/F_{min}$ = 0.12) (Figures 2b, S5b, S6c, Tables S2 and S3). In addition, some insertions unique to cpFusionRed were identified, such as Pro17 ($\Delta F/F_{min}$ = 0.16), Glu170 ($\Delta F/F_{min}$ = 0.11), and Asn172 ($\Delta F/F_{min}$ = 0.15). These results suggest that the use of different FPs may lead to the identification of different functional insertion sites (Figure S7).[15]

We attempted to employ the same strategy to discover functional biosensors based on the insertion of cpmKelly2 (derived from FR-GECO1).[16,17] However, this effort yielded predominantly dim variants that did not exhibit significant L-lactate-dependent changes in fluorescence. This suggests that cpmKelly2 may not be particularly amenable to the development of some SFPBs.

Random Insertions of cpmApple and cpFusionRed into a Spermidine-Binding Protein. To further explore the end-modified transposon strategy, we next attempted to identify prototype SFPBs for spermidine using *E. coli* PotD, a periplasmic binding protein involved in the polyamine transport system.[18,19] We used both Mu-cpmApple and Mu-cpFusionRed to create libraries of cpRFP insertions into PotD lacking its signal peptide (see Table S1 for sequence and residue numbering). For each library, we picked 1140 fluorescent variants (3× the theoretical number of possible insertions in 326 amino acids) from >30,000 colonies screened. Each of these variants was tested for their fluorescence response to 10 mM spermidine.

A total of 144 variants from each library, exhibiting superior fluorescence intensity and/or $\Delta F/F_{min}$, were subject to further in vitro characterization and sequencing. Each variant was cultured and protein extracted to be tested in buffers with and without 10 mM spermidine. Notably, both libraries revealed insertion sites with substantial responses to spermidine (Figures 2c, S8 and Table S2). Particularly noteworthy was a cpmApple insertion at Pro18 in PotD which gave a $\Delta F/F_{min}$ of 1.7 and a K_d for spermidine of 30 μM. For the cpFusionRed library, insertion at Gly118 gave a $\Delta F/F_{min}$ of 0.50 (K_d = 2.0 mM) and insertion at Thr268 gave a $\Delta F/F_{min}$ of 1.2 (K_d = 0.68 mM). Interestingly, some regions, including Pro18, served as common hotspots for both RFPs (Figure 2d). This validation of PotD as a suitable spermidine-binding domain sets the stage for further optimization to produce a high-performance biosensor (Figure S9 and Table S3).

Development of an miRFP680-Based Fluorescent Ca^{2+} Biosensor. In principle, NIR-genetically encoded Ca^{2+} indicators (NIR-GECIs) should offer advantages, such as lower background autofluorescence and deeper tissue fluorescence imaging, relative to more blue-shifted indicators.[20,21] We have previously reported several NIR-GECIs including the first- and second-generation NIR-GECOs,[22,23] and a blue-shifted version,[24] based on the insertion of a calmodulin (CaM)-RS20 Ca^{2+}-binding domain into the monomeric infrared FP (mIFP),[25] which employs a covalently attached biliverdin (BV) as a chromophore.[26] We will generally refer to such proteins as BV-FPs. Unfortunately, the utility of the NIR-GECO series is hindered by their suboptimal brightness during in vivo imaging, which is likely attributed to both the low intracellular concentration of BV and the low efficiency of covalent attachment of the protein to BV.[27,28] We reasoned that such limitations of the NIR-GECO series may be inherited from the mIFP template, which has actually been demonstrated to be one of the dimmer BV-FPs (Figure S10a).[29] Furthermore, we reasoned that developing a third-generation NIR-GECO from one of the brightest BV-FPs (miRFP680),[29] with the assistance of end-modified transposons, might enable us to overcome these limitations.

https://doi.org/10.1021/acssensors.4c00727
ACS Sens. 2024, 9, 3394−3402

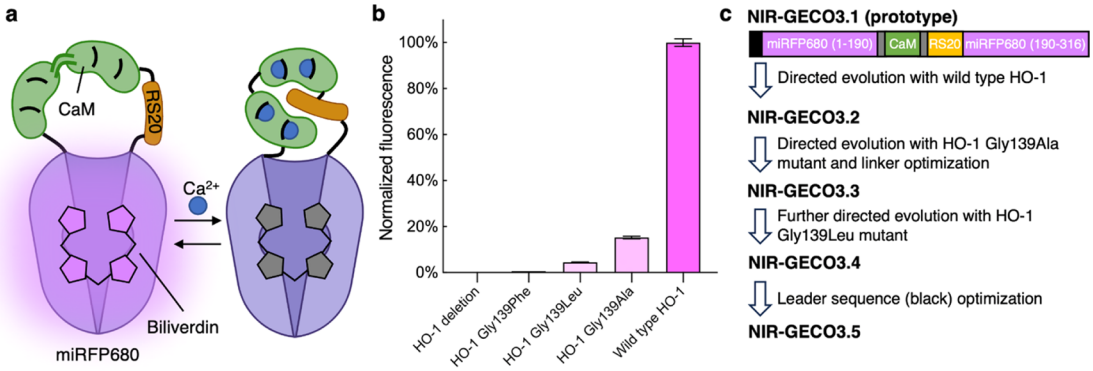

Figure 3. Development of NIR-GECO3 via directed evolution. (a) Schematic representation of the structure and response of NIR-GECO3 variants. (b) Relative fluorescent brightnesses of miRFP680 coexpressed with various HO-1 mutants, normalized to wild-type HO-1. (c) Genealogy of NIR-GECO3 variants.

To discover functional prototypes for a third-generation NIR-GECO, we created an end-modified Mu-CaM-RS20 transposon (Figure 1a) to enable insertion of CaM-RS20 domain into miRFP680 with a linker of one residue at the N-terminal end and no residues at the C-terminal end. Following methods identical to those described in previous sections, we picked approximately 800 fluorescent variants that were screened for response to Ca^{2+}. As we had done previously,[24] screening was performed with the coexpression of heme oxygenase-1 (HO-1) to produce BV in *E. coli*. Somewhat to our disappointment, the largest fluorescence change observed was a 15% reduction in fluorescence in response to 39 μM Ca^{2+} for the variant with CaM-RS20 inserted at Val190 (Figures 3a and S10b). This variant was designated as NIR-GECO3.1.

To improve the brightness and fluorescence response of NIR-GECO3.1, we performed 10 rounds of iterative directed evolution which led to NIR-GECO3.2 with a $\Delta F/F_{min}$ of 1.2 and higher molecular brightness (Table S4). At this point, we modified our screening strategy and, in addition to targeting a larger $\Delta F/F_{min}$, we also focused on improving the efficiency of BV binding. We had come to suspect that HO-1 was producing BV concentrations in *E. coli* that were much higher than what is typically present in mammalian cells. Accordingly, there was no selective pressure for efficient BV conjugation at physiologically relevant concentrations. To address this concern, we explored the use of previously reported HO-1 Gly139 mutants displaying diminished enzymatic activity,[30] which should result in lower BV production in *E. coli*. To assess their relative activity, we coexpressed these HO-1 mutants with miRFP680 and measured miRFP680 fluorescence (Figure 3b). For the Gly139Ala, Gly139Leu, and Gly139Phe mutants, we found that the relative fluorescence brightness of coexpressed miRFP680 was 15, 4.5%, and undetectable, respectively, relative to wild-type HO-1 coexpressed with miRFP680. Taking advantage of the lower BV concentrations, we undertook several additional rounds of directed evolution (Figure 3c) using the HO-1 Gly139Ala mutant (to produce NIR-GECO3.3 with $\Delta F/F_{min}$ of 4.0) followed by several more rounds using HO-1 Gly139Leu (to produce NIR-GECO3.4 with $\Delta F/F_{min}$ of 7.5). Serendipitously, we had discovered that modifications to the FLAG epitope within the leader sequence significantly influenced performance. Screening of libraries in which the residues of the FLAG epitope were randomized led to the identification of NIR-GECO3.5 with $\Delta F/F_{min}$ of 10 (320% of the molecular brightness of NIR-GECO3.2) (Figures 3c, S11 and Table S4).

Characterization of NIR-GECO3 Variants as Purified Proteins. We characterized NIR-GECO3 variants as purified proteins (Table S4), paying particular attention to NIR-GECO3.5 because it was the final end-product of the development process. Notably, purified NIR-GECO3.5 was distinguished by its substantial fluorescence response ($\Delta F/F_{min}$ = 10) and relatively high molecular brightness in the Ca^{2+} unbound state (Figure 4a and Table S4). Upon Ca^{2+} binding, the maximum extinction coefficient (at 656 nm) of NIR-GECO3.5 substantially decreased, which explains about half of the observed change in fluorescence (Figure 4b). The remainder of the observed change in fluorescence is attributable to a decrease in quantum yield upon Ca^{2+} binding (Table S4). We speculate that two or more isomers of BV could coexist in both the (−) and (+) states, and a shift in their relative proportions could explain the changes in both extinction coefficients and fluorescence quantum yields. We determined that NIR-GECO3.5 has an apparent K_d for Ca^{2+} of 298 nM, similar to that of the other NIR-GECO3 variants (Figure 4c). Two-photon spectral analysis revealed that there is an excitation peak for NIR-GECO3.5 at 1220 nm in the Ca^{2+}-free state (Figure 4d) and that the two-photon brightness decreases upon binding to Ca^{2+}.

To determine the kinetics of BV binding in vitro, we purified the protein in the BV-free state and then used absorbance spectroscopy to monitor BV binding (Figure 4e). Binding was very slow and continued for over 24 h with NIR-GECO3.5 exhibiting a rate that was intermediate between NIR-GECO1 (ref 22) and NIR-GECO2 (ref 23). Finally, by analyzing the pH sensitivity of NIR-GECO3.5, we determined that it exhibits a bell-shaped fluorescence response with pK_a values around 4 and 8.5, similar to that of other NIR-GECOs (Figure 4f).

Characterization of NIR-GECO3 Variants in Cultured Cells. To determine if the NIR-GECO3 variants functioned as expected in cultured cells, we performed time-lapse fluorescence microscopy of transfected HeLa cells. To determine the maximum and minimum fluorescence intensity in cells, we treated with ionomycin/EGTA to fully deplete Ca^{2+}, and with ionomycin/Ca^{2+} to saturate the NIR-GECO3 variants (Figures 4g and S12). Consistent with results using purified proteins (Table S4), NIR-GECO3.5 gave a maximum fluorescence change ($\Delta F/F_{min}$ = 14) that was substantially larger than the other NIR-GECO variants. Under these conditions, the cell-based Ca^{2+}-induced fluorescence change of NIR-GECO3.5 was

https://doi.org/10.1021/acssensors.4c00727
ACS Sens. 2024, 9, 3394−3402

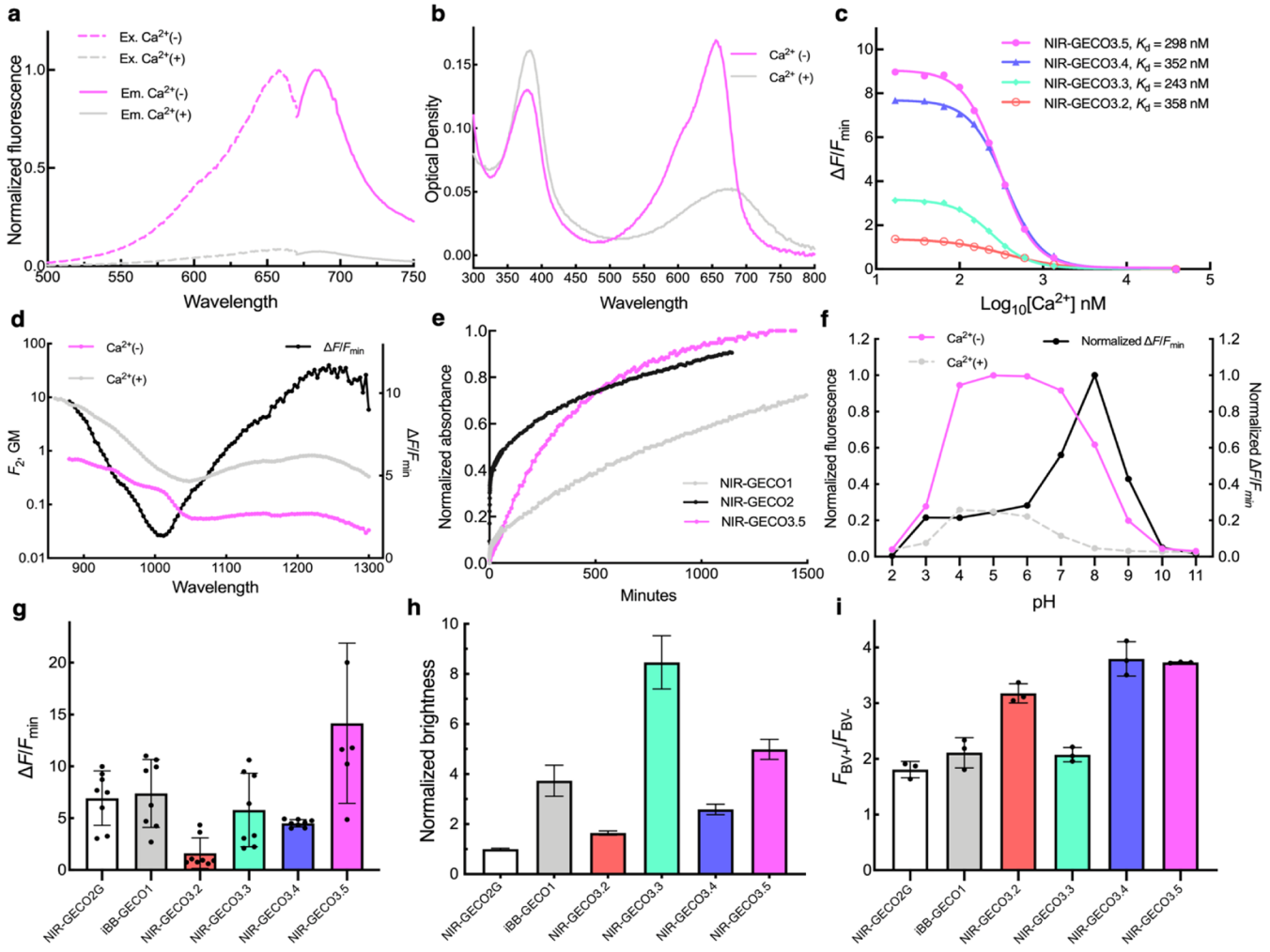

Figure 4. Characterization of NIR-GECO3 variants. (a) Excitation (emission at 710 nm) and emission spectra (excitation at 630 nm) of purified NIR-GECO3.5 protein in the presence (39 μM) and absence of Ca^{2+}. (b) Absorbance spectra of purified NIR-GECO3.5 protein in the presence (39 μM) and absence of Ca^{2+}. (c) $\Delta F/F_{min}$ as a function of Ca^{2+} concentration for NIR-GECO3 variants. (d) Two-photon excitation spectra of purified NIR-GECO3.5 protein in the presence (39 μM) and absence of Ca^{2+}. $\Delta F/F_{min}$ is indicated on the right axis. GM, Goeppert-Mayer units. (e) BV binding kinetics of purified NIR-GECO1, NIR-GECO2, and NIR-GECO3.5 proteins. The peak absorbance (at 680 nm for NIR-GECO1/2 and 660 nm for NIR-GECO3.5) is plotted against time and normalized to the maximum absorbance (obtained by fitting the data to an exponential curve). (f) pH titration of purified NIR-GECO3.5 protein in the presence (39 μM) and absence of Ca^{2+}. $\Delta F/F_{min}$ is represented on the right axis. Values are normalized to their maximum. (g) $\Delta F/F_{min}$ of NIR-GECO3 variants in HeLa cells where F is the fluorescence with ionomycin/EGTA (2 μM + 1 mM) and F_{min} is the fluorescence with ionomycin/Ca^{2+} (2 μM + 4 mM) (n = 8 cells per group). (h) Normalized effective brightness of NIR-GECO3 variants, relative to NIR-GECO2G, measured from approximately 2000 cells transfected with NIR-GECO-P2A-EGFP-3NLS (3 technical replicates) using flow cytometry. Data represents the median value. (i) F_{BV+}/F_{BV-} value of NIR-GECO3 variants. The F_{BV+} group had 12.5 μM BV added 2 h before measurement. Flow cytometry of approximately 2000 cells transfected as in (h), with brightnesses relative to EGFP.

also larger than that of iBB-GECO1 and NIR-GECO2G.[23,24] iBB-GECO1 was selected as the control due to it having a similar emission peak (668 nm) with the NIR-GECO3 variants (Table S4). Consistent with the in vitro results, of all of the NIR-GECO variants investigated, NIR-GECO3.5 exhibited the largest intensiometric Ca^{2+}-induced fluorescence change. We also determined that the NIR-GECO3 variants could be effectively used to monitor histamine-induced Ca^{2+} oscillations in HeLa cells (Figure S13).

Flow cytometry analysis was performed to assess the brightness of NIR-GECO3 variants expressed in HeLa cells using excitation at 640 nm and emission at 670/14 nm (Figure 4h). All NIR-GECO3 variants were substantially brighter than NIR-GECO2G, with the brightest variants being NIR-GECO3.5 (5.0× brighter) and NIR-GECO3.3 (8.5× brighter). To determine if the enhanced brightness was attributable to more efficient BV binding, we compared the brightness of variants in the presence versus the absence of exogenous BV. A lower fluorescence enhancement ratio (F_{BV+}/F_{BV-}) would suggest more efficient BV binding under normal cellular conditions. We had previously found that treatment of cells expressing NIR-GECO1 with 25 μM BV for 3 h yielded an approximately 5× increase in the brightness,[22] and Shemetov et al. reported 8.1× the brightness with 25 μM BV for 24 h.[31] In the current work, we found ratios ranging from 2.1 for NIR-GECO3.3 to 3.8 for NIR-GECO3.4 (Figure 4i). These ratios are much less than those reported for NIR-GECO1, suggesting that our strategy of screening using HO-1 mutants was successful in increasing the efficiency of BV conjugation. It is worth noting that the F_{BV+}/F_{BV-} ratios for NIR-GECO2G and iBB-GECO1 are 1.8 and 2.1, respectively, suggesting that efficient BV binding can also be achieved without the use of

https://doi.org/10.1021/acssensors.4c00727
ACS Sens. 2024, 9, 3394−3402

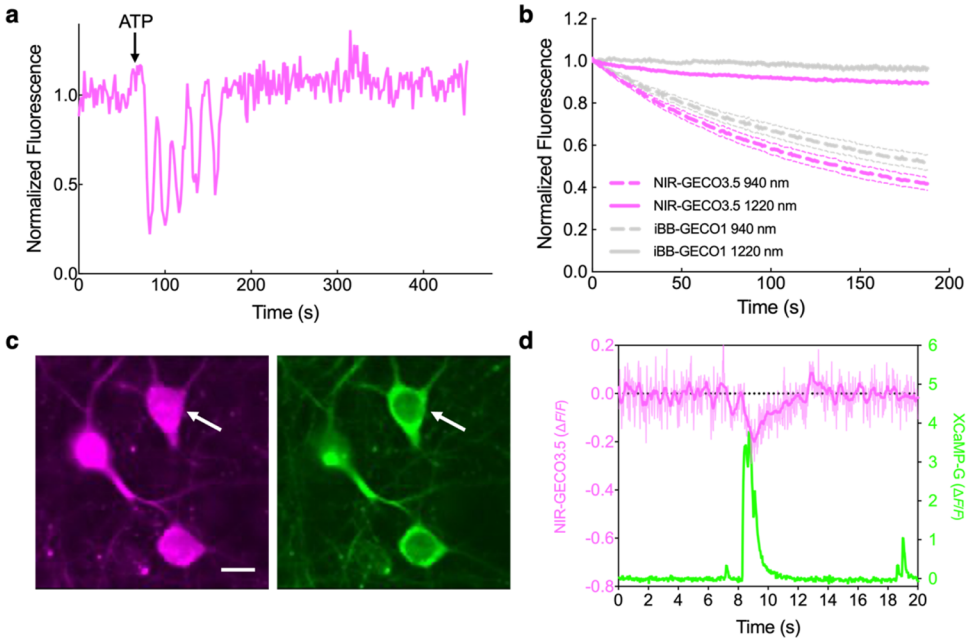

Figure 5. Two-photon imaging of NIR-GECO3.5. (a) Representative trace of NIR-GECO3.5 response in a HEK293T cell in response to 100 μM ATP, using 1220 nm excitation. (b) Photobleaching curves for NIR-GECO3.5 and iBB-GECO1 in HEK293T cells at both 940 and 1220 nm excitation. Laser power was adjusted so that the obtained fluorescence intensity was similar level (Figure S14c). Areas between thinner dotted lines represent s.e.m (n = 57 for NIR-GECO3.5 at 940 nm, n = 75 for NIR-GECO3.5 at 1220 nm, n = 55 for iBB-GECO1 at 940 nm, n = 55 for iBB-GECO1 at 1220 nm). (c) Representative two-photon excitation (940 nm) images of NIR-GECO3.5 (left) and XCaMP-G (right) expressed in live mouse brain and imaged in slices. Scale bar, 10 μm. (d) Representative time courses of $\Delta F/F$ for in vivo imaging of spontaneous neuronal activity with both NIR-GECO3.5 and XCaMP-G. A Savitzky-Golay filter was applied to NIR-GECO3.5, and a median filter was applied to XCaMP-G.

HO-1 mutants.[23,24] Nevertheless, we recommend directed evolution using HO-1 mutants with decreased activity as an efficient approach to develop brighter BV-FPs and BV-FP-based SFPBs.

Two-Photon Fluorescence Imaging of NIR-GECO3 Variants. To truly take advantage of the longer wavelength fluorescence of an NIR-GECI for imaging deep into brain tissue, it would be ideal to use two-photon excitation. Our in vitro characterization had revealed that NIR-GECO3.5 underwent most efficient two-photon excitation at wavelengths of about 900 and 1200 nm (Figure 4d). To determine if two-photon excitation could be used to image the Ca^{2+}-dependent response of NIR-GECO3 in cells, HEK293T cells were transfected with pCAG-NIR-GECO3.5 and stimulated with 100 μM adenosine triphosphate (ATP) while being imaged with 940 and 1220 nm excitation (Figures 5a and S14a). We observed the expected oscillatory changes in fluorescence, consistent with our expectations of NIR-GECO3.5's Ca^{2+}-responsiveness to cellular Ca^{2+} dynamics. Excitation at the two wavelengths resulted in similar fluorescence changes (Figure S14b), though illumination at 940 nm led to more rapid photobleaching for both NIR-GECO3.5 and iBB-GECO1 (Figures 5b and S14c,d).

To explore if NIR-GECO3.5 could be useful for in vivo imaging of neural activity, the genes encoding NIR-GECO3.5 and XCaMP-G[32] were expressed in layer 2/3 (L2/3) of mouse cortex using in utero electroporation. In vivo two-photon imaging (940 nm) revealed detectable NIR-GECO3.5 fluorescence without addition of exogenous BV or coexpression of HO-1 (Figure 5c). Simultaneous in vivo imaging of NIR-GECO3.5 and XCaMP-G (as a positive control) enabled us to observe the neuronal-activity-dependent NIR fluorescence changes (Figure 5d). Analysis of the cumulative SNR data revealed that NIR-GECO3.5 exhibits superior SNR compared to the benchmark iBB-GECO1 (Figure S15).

CONCLUSIONS

In this work, we described an effective strategy for the discovery of red fluorescent SFPB prototypes and provided examples of using this strategy with two different cpRFPs (cpmApple and cpFusionRed) and three different binding domains (L-lactate-, spermidine-, and Ca^{2+}-binding domains), and with two different topologies (i.e., insertion of a fluorescing domain into a binding domain, and insertion of a binding domain into an FP domain). The particular challenge that we set out to overcome in this work was how to create libraries of prototypes in which the allosteric coupling between the binding domain and the fluorescing domain is maximized. We ultimately achieved this by using end-modified transposons that leave linkers as short as a single residue, or no residues at all, between the two domains. We are confident that this end-modified transposon method will be broadly useful for the development of new and improved SFPBs which, in turn, will be applicable to a wide variety of biological problems.

Although the main focus of this work is the end-modified transposon method, in the course of demonstrating this technology we have produced promising biosensor prototypes for L-lactate (i.e., cpmApple inserted into LldR-LBD at Pro112) and spermidine (i.e., cpmApple inserted into PotD at Pro18), as well as the highly optimized miRFP680-based NIR-GECO3 series of Ca^{2+} biosensors. Among the NIR-GECO3 series, the NIR-GECO3.5 variant stands out as particularly promising because of its balance between brightness and fluorescent response. Preliminary imaging experiments in cell culture and in vivo suggest that NIR-GECO3.5 does not represent a great leap forward from existing NIR-

https://doi.org/10.1021/acssensors.4c00727
ACS Sens. 2024, 9, 3394−3402

GECOs. However, it does match or exceed existing NIR-GECOs in certain criteria (i.e., effective brightness and $\Delta F/F_{min}$ in HeLa cells, SNR in vivo), and in this regard, it serves as both a useful new addition to the family of NIR-GECIs and a validation of the effectiveness of our end-modified transposon engineering strategy.

■ ASSOCIATED CONTENT

Supporting Information

The Supporting Information is available free of charge at https://pubs.acs.org/doi/10.1021/acssensors.4c00727.

Materials and methods; transposon-mediated insertion (Figure S1); LldR-LBD and PotD insertions (Figures S2−S9); NIR-GECO3 development and characterization (Figures S10−S15); sequences of proteins used in this work (Table S1); variants in LldR-LBD and PotD libraries (Tables S2 and S3); detailed summary of NIR-GECO3 properties (Table S4) (PDF)

■ AUTHOR INFORMATION

Corresponding Author

Robert E. Campbell − *Department of Chemistry, Graduate School of Science, The University of Tokyo, Tokyo 113-0033, Japan; CERVO Brain Research Center and Department of Biochemistry, Microbiology, and Bioinformatics, Université Laval, Québec, Québec G1 V 0A6, Canada;* orcid.org/0000-0003-0604-092X; Email: campbell@chem.s.u-tokyo.ac.jp

Authors

Fu Chai − *Department of Chemistry, Graduate School of Science, The University of Tokyo, Tokyo 113-0033, Japan*

Hajime Fujii − *Department of Neurochemistry, Graduate School of Medicine, The University of Tokyo, Tokyo 113-0033, Japan*

Giang N. T. Le − *Department of Chemistry, University of Toronto, Toronto, Ontario M5S 3H6, Canada*

Chang Lin − *College of Chemistry and Molecular Engineering, Peking University, Beijing 100871, China;* orcid.org/0000-0003-0445-6964

Keisuke Ota − *Department of Neurochemistry, Graduate School of Medicine, The University of Tokyo, Tokyo 113-0033, Japan*

Karl Matthew Lin − *Department of Chemistry, Graduate School of Science, The University of Tokyo, Tokyo 113-0033, Japan*

Lam M. T. Pham − *Department of Chemistry, University of Toronto, Toronto, Ontario M5S 3H6, Canada*

Peng Zou − *College of Chemistry and Molecular Engineering, Peking University, Beijing 100871, China;* orcid.org/0000-0002-9798-5242

Mikhail Drobizhev − *Department of Microbiology and Cell Biology, Montana State University, Bozeman, Montana 59717, United States*

Yusuke Nasu − *Department of Chemistry, Graduate School of Science, The University of Tokyo, Tokyo 113-0033, Japan; PRESTO, Japan Science and Technology Agency, Tokyo 102-0075, Japan;* orcid.org/0000-0002-3193-9104

Takuya Terai − *Department of Chemistry, Graduate School of Science, The University of Tokyo, Tokyo 113-0033, Japan;* orcid.org/0000-0002-3425-3589

Haruhiko Bito − *Department of Neurochemistry, Graduate School of Medicine, The University of Tokyo, Tokyo 113-0033, Japan*

Complete contact information is available at: https://pubs.acs.org/10.1021/acssensors.4c00727

Author Contributions

○H.F., G.N.T.L., C.L., and K.O. contributed equally to this work. F.C.: development and characterization of NIR-GECO3; data analysis; figure preparation; writing of original manuscript draft; and editing. H.F.: two-photon imaging; data analysis; writing of the methods section; and editing. G.N.T.L.: measurement of biliverdin binding kinetics; data analysis; writing of the methods section; and editing. C.L.: flow cytometry measurements; data analysis; writing of the methods section; and editing. K.O.: two-photon imaging; data analysis; writing of the methods section; and editing. K.M.L.: assistance with directed evolution of NIR-GECO3 and editing. L.M.T.P.: measurement of biliverdin binding kinetics. P.Z.: funding acquisition; supervision; and editing. M.D.: measurement of two-photon spectra; data analysis; writing of the methods section; funding acquisition; and editing. Y.N.: funding acquisition; supervision; and editing. T.T.: funding acquisition; supervision; and editing. H.B.: funding acquisition; supervision; and editing. R.E.C.: project conception; funding acquisition; supervision; and editing. All authors read and approved the final manuscript.

Notes

The authors declare no competing financial interest.

■ ACKNOWLEDGMENTS

The authors are grateful to Dr. Daniel Razansky, Dr. Michael Arand, and Dr. G. Andrew Woolley for technical support and access to instrumentation. Work at the University of Tokyo was primarily supported by Japan Society for the Promotion of Science (JSPS) Grants-in-Aid for Scientific Research S (KAKENHI) 19H05633 and NIH BRAIN Initiative (1R01NS126102-01; PI Shy Shoham) to R.E.C. F.C. was supported by Japan Science and Technology Agency (JST) SPRING (JPMJSP2108). G.N.T.L. was supported by the NSERC CREATE Advanced Protein Engineering Training, Internships, Courses, and Exhibition (APRENTICE) program. M.D. was supported by an NIH/NINDS BRAIN Initiative grant (U24NS109107). K.M.L. was supported by the Fulbright U.S. Student Program and the Japan-U.S. Education Commission. Y.N. acknowledges the support of JSPS Grants-in-Aid for Early-Career Scientists (21K14738) and JST PRESTO (JPMJPR22E9). T.T. acknowledges the support of JSPS KAKENHI (18H02103, 21H00273, and 23H02101). P.Z. was supported by the Ministry of Science and Technology of China (2022YFA1304700) and the National Natural Science Foundation of China (32088101). H.F. was supported by JSPS KAKENHI (23K06344). H.B. was supported by JSPS KAKENHI (JP22H05160, 22H00432) and AMED (Brain/MINDS JP19dm0207079 and SICORP 22jm0210098).

■ REFERENCES

(1) Greenwald, E. C.; Mehta, S.; Zhang, J. Genetically Encoded Fluorescent Biosensors Illuminate the Spatiotemporal Regulation of Signaling Networks. *Chem. Rev.* **2018**, *118*, 11707−11794.

(2) Frei, M. S.; Mehta, S.; Zhang, J. Next-Generation Genetically Encoded Fluorescent Biosensors Illuminate Cell Signaling and Metabolism. *Annu. Rev. Biophys.* **2024**, *53*, 275−297.

(3) Nasu, Y.; Shen, Y.; Kramer, L.; Campbell, R. E. Structure- and Mechanism-Guided Design of Single Fluorescent Protein-Based Biosensors. *Nat. Chem. Biol.* **2021**, *17*, 509−518.
(4) Akerboom, J.; Chen, T.-W. W.; Wardill, T. J.; Tian, L.; Marvin, J. S.; Mutlu, S.; Calderón, N. C.; Esposti, F.; Borghuis, B. G.; Sun, X. R.; et al. Optimization of a GCaMP Calcium Indicator for Neural Activity Imaging. *J. Neurosci.* **2012**, *32*, 13819−13840.
(5) Nadler, D. C.; Morgan, S.-A.; Flamholz, A.; Kortright, K. E.; Savage, D. F. Rapid Construction of Metabolite Biosensors Using Domain-Insertion Profiling. *Nat. Commun.* **2016**, *7*, No. 12266.
(6) Kinney, J. B.; Murugan, A.; Callan, C. G., Jr; Cox, E. C. Using Deep Sequencing to Characterize the Biophysical Mechanism of a Transcriptional Regulatory Sequence. *Proc. Natl. Acad. Sci. U.S.A.* **2010**, *107*, 9158−9163.
(7) Koberstein, J. N.; Stewart, M. L.; Mighell, T. L.; Smith, C. B.; Cohen, M. S. A Sort-Seq Approach to the Development of Single Fluorescent Protein Biosensors. *ACS Chem. Biol.* **2021**, *16*, 1709−1720.
(8) Kostyuk, A. I.; Demidovich, A. D.; Kotova, D. A.; Belousov, V. V.; Bilan, D. S. Circularly Permuted Fluorescent Protein-Based Indicators: History, Principles, and Classification. *Int. J. Mol. Sci.* **2019**, *20*, No. 4200, DOI: 10.3390/ijms20174200.
(9) Zhao, Y.; Araki, S.; Wu, J.; Teramoto, T.; Chang, Y.-F.; Nakano, M.; Abdelfattah, A. S.; Fujiwara, M.; Ishihara, T.; Nagai, T.; Campbell, R. E. An Expanded Palette of Genetically Encoded Ca^{2+} Indicators. *Science* **2011**, *333*, 1888−1891, DOI: 10.1126/science.1208592.
(10) Shen, Y.; Dana, H.; Abdelfattah, A. S.; Patel, R.; Shea, J.; Molina, R. S.; Rawal, B.; Rancic, V.; Chang, Y.-F.; Wu, L.; et al. A Genetically Encoded Ca2+ Indicator Based on Circularly Permutated Sea Anemone Red Fluorescent Protein EqFP578. *BMC Biol.* **2018**, *16*, No. 9, DOI: 10.1186/s12915-018-0480-0.
(11) Lee, I.; Harshey, R. M. The Conserved CA/TG Motif at Mu Termini: T Specifies Stable Transpososome Assembly. *J. Mol. Biol.* **2003**, *330*, 261−275.
(12) Gao, Y.-G.; Suzuki, H.; Itou, H.; Zhou, Y.; Tanaka, Y.; Wachi, M.; Watanabe, N.; Tanaka, I.; Yao, M. Structural and Functional Characterization of the LldR from Corynebacterium Glutamicum: A Transcriptional Repressor Involved in L-Lactate and Sugar Utilization. *Nucleic Acids Res.* **2008**, *36*, 7110−7123.
(13) Hario, S.; Le, G. N. T.; Sugimoto, H.; Takahashi-Yamashiro, K.; Nishinami, S.; Toda, H.; Li, S.; Marvin, J. S.; Kuroda, S.; Drobizhev, M.; et al. High-Performance Genetically Encoded Green Fluorescent Biosensors for Intracellular l-Lactate. *ACS Cent. Sci.* **2024**, *10*, 402−416.
(14) Nasu, Y.; Aggarwal, A.; Le, G. N. T.; Vo, C. T.; Kambe, Y.; Wang, X.; Beinlich, F. R. M.; Lee, A. B.; Ram, T. R.; Wang, F.; et al. Lactate Biosensors for Spectrally and Spatially Multiplexed Fluorescence Imaging. *Nat. Commun.* **2023**, *14*, No. 6598.
(15) Jumper, J.; Evans, R.; Pritzel, A.; Green, T.; Figurnov, M.; Ronneberger, O.; Tunyasuvunakool, K.; Bates, R.; Žídek, A.; Potapenko, A.; et al. Highly Accurate Protein Structure Prediction with AlphaFold. *Nature* **2021**, *596*, 583−589.
(16) Wannier, T. M.; Gillespie, S. K.; Hutchins, N.; McIsaac, R. S.; Wu, S.-Y.; Shen, Y.; Campbell, R. E.; Brown, K. S.; Mayo, S. L. Monomerization of Far-Red Fluorescent Proteins. *Proc. Natl. Acad. Sci. U.S.A.* **2018**, *115*, E11294−E11301.
(17) Dalangin, R.; Drobizhev, M.; Molina, R. S.; Aggarwal, A.; Patel, R.; Abdelfattah, A. S.; Zhao, Y.; Wu, J.; Podgorski, K.; Schreiter, E. R.et al. Far-Red Fluorescent Genetically Encoded Calcium Ion Indicators *bioRxiv* 2020 DOI: 10.1101/2020.11.12.380089.
(18) Sugiyama, S.; Vassylyev, D. G.; Matsushima, M.; Kashiwagi, K.; Igarashi, K.; Morikawa, K. Crystal Structure of PotD, the Primary Receptor of the Polyamine Transport System in *Escherichia Coli*. *J. Biol. Chem.* **1996**, *271*, 9519−9525.
(19) Kashiwagi, K.; Miyamoto, S.; Nukui, E.; Kobayashi, H.; Igarashi, K. Functions of PotA and PotD Proteins in Spermidine-Preferential Uptake System in *Escherichia Coli*. *J. Biol. Chem.* **1993**, *268*, 19358−19363.
(20) Frangioni, J. V. In Vivo Near-Infrared Fluorescence Imaging. *Curr. Opin. Chem. Biol.* **2003**, *7*, 626−634.
(21) Shcherbakova, D. M.; Verkhusha, V. V. Near-Infrared Fluorescent Proteins for Multicolor in Vivo Imaging. *Nat. Methods* **2013**, *10*, 751−754.
(22) Qian, Y.; Piatkevich, K. D.; Mc Larney, B.; Abdelfattah, A. S.; Mehta, S.; Murdock, M. H.; Gottschalk, S.; Molina, R. S.; Zhang, W.; Chen, Y.; et al. A Genetically Encoded Near-Infrared Fluorescent Calcium Ion Indicator. *Nat. Methods* **2019**, *16*, 171−174.
(23) Qian, Y.; Cosio, D. M. O.; Piatkevich, K. D.; Aufmkolk, S.; Su, W.-C.; Celiker, O. T.; Schohl, A.; Murdock, M. H.; Aggarwal, A.; Chang, Y.-F.; et al. Improved Genetically Encoded Near-Infrared Fluorescent Calcium Ion Indicators for in Vivo Imaging. *PLoS Biol.* **2020**, *18*, No. e3000965.
(24) Hashizume, R.; Fujii, H.; Mehta, S.; Ota, K.; Qian, Y.; Zhu, W.; Drobizhev, M.; Nasu, Y.; Zhang, J.; Bito, H.; Campbell, R. E. A Genetically Encoded Far-Red Fluorescent Calcium Ion Biosensor Derived from a Biliverdin-Binding Protein. *Protein Sci.* **2022**, *31*, No. e4440.
(25) Yu, D.; Baird, M. A.; Allen, J. R.; Howe, E. S.; Klassen, M. P.; Reade, A.; Makhijani, K.; Song, Y.; Liu, S.; Murthy, Z.; et al. A Naturally Monomeric Infrared Fluorescent Protein for Protein Labeling in Vivo. *Nat. Methods* **2015**, *12*, 763−765.
(26) Shu, X.; Royant, A.; Lin, M. Z.; Aguilera, T. A.; Lev-Ram, V.; Steinbach, P. A.; Tsien, R. Y. Mammalian Expression of Infrared Fluorescent Proteins Engineered from a Bacterial Phytochrome. *Science* **2009**, *324*, 804−807.
(27) Kobachi, K.; Kuno, S.; Sato, S.; Sumiyama, K.; Matsuda, M.; Terai, K. Biliverdin Reductase-A Deficiency Brighten and Sensitize Biliverdin-Binding Chromoproteins. *Cell Struct. Funct.* **2020**, *45*, 131−141.
(28) Montecinos-Franjola, F.; Lin, J. Y.; Rodriguez, E. A. Fluorescent Proteins for in Vivo Imaging, Where's the Biliverdin? *Biochem. Soc. Trans.* **2020**, *48*, 2657−2667.
(29) Matlashov, M. E.; Shcherbakova, D. M.; Alvelid, J.; Baloban, M.; Pennacchietti, F.; Shemetov, A. A.; Testa, I.; Verkhusha, V. V. A Set of Monomeric Near-Infrared Fluorescent Proteins for Multicolor Imaging across Scales. *Nat. Commun.* **2020**, *11*, No. 239.
(30) Liu, Y.; Lightning, L. K.; Huang, H.; Moënne-Loccoz, P.; Schuller, D. J.; Poulos, T. L.; Loehr, T. M.; de Montellano, P. R. O. Replacement of the Distal Glycine 139 Transforms Human Heme Oxygenase-1 into a Peroxidase. *J. Biol. Chem.* **2000**, *275*, 34501−34507, DOI: 10.1074/jbc.M004245200.
(31) Shemetov, A. A.; Monakhov, M. V.; Zhang, Q.; Canton-Josh, J. E.; Kumar, M.; Chen, M.; Matlashov, M. E.; Li, X.; Yang, W.; Nie, L.; et al. A Near-Infrared Genetically Encoded Calcium Indicator for in Vivo Imaging. *Nat. Biotechnol.* **2021**, *39*, 368−377.
(32) Inoue, M.; Takeuchi, A.; Manita, S.; Horigane, S.-I.; Sakamoto, M.; Kawakami, R.; Yamaguchi, K.; Otomo, K.; Yokoyama, H.; Kim, R.; et al. Rational Engineering of XCaMPs, a Multicolor GECI Suite for In Vivo Imaging of Complex Brain Circuit Dynamics. *Cell* **2019**, *177*, 1346−1360.e24.

https://doi.org/10.1021/acssensors.4c00727
ACS Sens. 2024, 9, 3394−3402